NANO LETTERS

Letter

pubs.acs.org/NanoLett

# Observation of Localized Vibrational Modes of Graphene Nanodomes by Inelastic Atom Scattering

D. Maccariello,[†,‡] A. Al Taleb,[‡] F. Calleja,[†] A. L. Vázquez de Parga,[†,‡,§,⊥] P. Perna,[†] J. Camarero,[†,‡,§,⊥] E. Gnecco,[†] D. Farías,[*,‡,§,⊥] and R. Miranda[†,‡,§,⊥]

[†]Instituto Madrileño de Estudios Avanzados en Nanociencia (IMDEA-Nanociencia), 28049 Madrid, Spain

[‡]Departamento de Física de la Materia Condensada, [§]Instituto de Ciencia de Materiales "Nicolás Cabrera", and [⊥]Condensed Matter Physics Center (IFIMAC), Universidad Autónoma de Madrid, 28049 Madrid, Spain

Supporting Information

**ABSTRACT:** Inelastic helium atom scattering (HAS) is suitable to determine low-energy (few meV) vibrations spatially localized on structures in the nanometer range. This is illustrated for the nanodomes that appear often on graphene (Gr) epitaxially grown on single crystal metal surfaces. The nature of the inelastic losses observed in Gr/Ru(0001) and Gr/Cu/Ru(0001) has been clarified by intercalation of Cu below the Gr monolayer, which decouples the Gr layer from the Ru substrate and changes substantially the out-of-plane, flexural phonon dispersion of epitaxial Gr, while maintaining the nanodomes and their localized vibrations. He diffraction proves that the Cu-intercalated Gr layer is well ordered structurally, while scanning tunneling microscopy reveals the persistence of the (slightly modified) periodic array of Gr nanodomes. A simple model explains the order of magnitude of the energy losses associated with the Gr nanodomes and their size dependence. The dispersionless, low-energy phonon branches may radically alter the transport of heat in intercalated Gr.

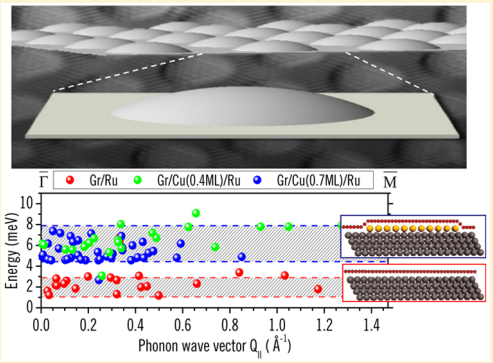


**KEYWORDS:** *Graphene, copper, ruthenium, phonons, STM, helium atom scattering*

Determining the low-energy electronic, mechanical, or magnetic excitations of nanostructures is a crucial step toward understanding their behavior and improving their functionalities, and techniques with extreme spatial resolution have been developed to this end. Thus, vibrational excitations of nanostructures down to individual molecules can be examined by inelastic scanning tunneling spectroscopy (STS),[1] local resonance frequencies can be extracted from noncontact atomic force microscopy and spectroscopy in ultra high vacuum,[2] or spin-flip transitions can be detected on single atoms by STS at very low temperatures.[3]

On the other side, the in-plane thermal conductivity of a solid in the diffusive regime is given by $\kappa = C\nu\lambda$, where C is the specific heat, $\nu$ is the phonon group velocity, and $\lambda$ is the phonon mean free path. The thermal conductivity of suspended graphene (Gr) is known to be exceptionally high, reaching 3000−5000 W mK$^{-1}$ at 300 K.[4] The specific heat of Gr is dominated by the lattice vibrations.[5] Free standing, suspended Gr has a lower branch of flexural phonons ZA, which may be suppressed or their dispersion radically altered by a substrate when depositing Gr on it. For instance, for Gr deposited on a silicon dioxide substrate, $\kappa$ is reduced to 600 W mK$^{-1}$ at 300 K.[4] In addition, scattering of the Gr phonons with the substrate phonons will also reduce substantially $\lambda$ (from 600 to 100 nm) and, accordingly, decrease the thermal conductivity. Therefore, modifications of ZA flexural phonon modes are crucial, and its determination is relevant to understand the thermal properties of epitaxial Gr grown on a variety of substrates.

Traditionally, the determination of surface phonon dispersion curves has been carried out by inelastic electron or helium atom scattering (HAS), the latter being the only accessible technique for ultralow (below 60 meV) energy phonons.[6] In the present work, we report that inelastic HAS can also detect vibrations localized on structures only a few nanometers in lateral size, specifically in the Gr nanodomes present in many periodically rippled epitaxial Gr monolayers such as Gr/Ru(0001) and Cu-intercalated Gr/Ru(0001). The intercalation of Cu removes other low-energy Gr vibrational modes and leaves only the vibrations localized on the nanodomes. Scanning tunneling microscopy (STM) has been used to characterize the intercalated system in the real space. The low energy vibration modes localized on the nanodomes may alter substantially the heat transport in epitaxial Gr.

Gr was epitaxially grown on Ru(0001) by thermal decomposition of ethylene at 1150 K.[7,8] Cu has been intercalated underneath the Gr layer following the procedure already reported for the Gr/Ni(111) system.[10,11] In brief, a nominal amount of Cu was evaporated at room temperature on

**Received:** April 23, 2015
**Revised:** November 23, 2015





DOI: 10.1021/acs.nanolett.5b02887
*Nano Lett.* XXXX, XXX, XXX−XXX

the Gr/Ru(0001) surface, which was afterward heated to 800 K. Before every intercalation experiment, the Cu evaporation rate was calibrated by looking at the first maximum of the He reflectivity during the deposition of Cu on clean Ru(0001).

The morphology of Gr/Ru(0001) is well-known,[7−9] while the one of Cu-intercalated Gr/Ru(0001) surface in the real space has been obtained by STM. Figure 1 shows two atomic

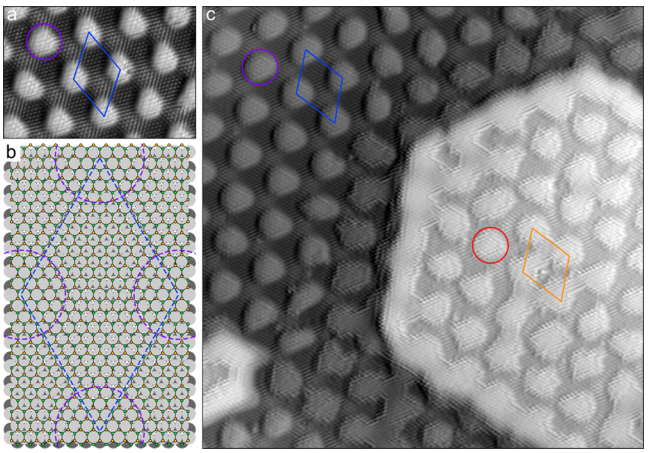


**Figure 1.** STM atomic resolution images recorded at 80 K on Gr/Ru(0001) (a) before and (c) after intercalation of 0.5 ML of Cu. (a) Before intercalation, 12 × 8 nm$^2$ area scanned at −5 mV and 100 pA. The unit cell of the moiré pattern resulting from the lattice mismatch between Gr and Ru(0001) is highlighted in blue. One of the corresponding "nanodome" regions (where all carbon atoms sit in three-fold positions of the Ru(0001) lattice) is marked in purple. (b) Schematic model of the atomic positions where dark and light gray circles represent the last two ruthenium layers. Green and orange circles correspond to the carbon atoms of each Gr sublattice. As in the image of panel a, the moiré cell and nanodome regions are marked in blue and purple, respectively. (c) After Cu intercalation, 30 × 30 nm$^2$ image scanned at −30 mV and 1 nA. Moving from the upper left corner to the lower right, a clean Gr/Ru region (dark) meets an intercalated one (brighter). The moiré cells are highlighted in blue and orange and the nanodome regions in purple and red, respectively.

resolution images recorded on a Ru(0001) sample partially covered by Gr before and after deposition of nominally 0.5 monolayer (ML) of Cu at 300 K and heating to 800 K. Figure 1, panel a and the upper left corner of panel c correspond to the epitaxial, periodically rippled Gr layer on Ru(0001), with its characteristic moiré pattern made of bright bumps (nanodomes) with an apparent vertical corrugation of 0.116 nm at this imaging voltage and separated by about 0.30 nm.[8] A schematic model of the corresponding atomic positions is presented in Figure 1, panel b. The lower right corner of Figure 1, panel c shows an area where Cu atoms have been intercalated between Gr and the Ru substrate. For these deposited amount and intercalation conditions, the intercalated area represents 18% of the total surface. Finally, the Gr free regions of the sample (not shown here, see Supporting Information) present a pseudomorphic, (1 × 1) Cu overlayer.[12,13]

The STM image with atomic resolution reproduced in Figure 1, panel c shows that the structural integrity of the Gr layer is preserved, and Gr extends continuously over both intercalated and nonintercalated regions. The lateral periodicity of the moiré pattern is identical in the Cu-intercalated Gr islands and in the pristine Gr/Ru(0001) regions. This indicates that the intercalated Cu islands are pseudomorphic with the Ru substrate, that is, the Cu−Cu distances are expanded to adjust the Ru−Ru distances in the substrate. This result is consistent with the behavior of the same system without Gr. Indeed, the epitaxial growth of Cu on Ru(0001) has been extensively studied, resulting in a deep understanding of the geometry and strain of the different layers.[14−21] For the sake of the present study, we note that the first monolayer grows psudomorphically, accumulating a tensile strain of 5.5%. Analysis of the STM line profiles (see Supporting Information) reveals that the apparent corrugation due to the moiré reconstruction in the intercalated areas has been reduced to 0.07 nm at this bias voltage, that is, approximately 40% lower than in the Gr/Ru(0001) regions for the same bias voltage. The apparent step height of the islands, 0.25 nm, indicates that the intercalated Cu layer is only one atom high. For higher coverages of Cu deposited, the intercalated area grows until it covers most of the surface. The real space imaging by STM allows to estimate the efficiency of the entire intercalation process with respect to the initially deposited amount of Cu, which turns out to be of the order of 33%. In the following, we will concentrate on two representative Cu-intercalated coverages, namely Gr/Cu(0.4 ML)/Ru and Gr/Cu(0.7 ML)/Ru.

Relevant information on the degree of long-range order in the intercalated systems has been obtained by measuring HAS angular distributions. Figure 2 shows the He-diffraction pattern

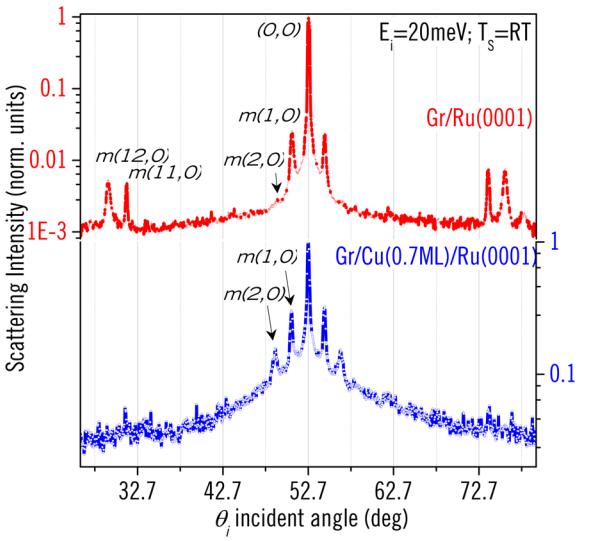


**Figure 2.** Normalized angular distributions (in logarithmic scales) of a beam of He atoms scattered by Gr/Ru(0001) (top) and Gr/Cu(0.7 ML)/Ru(0001) (bottom). The arrows indicate some significant changes in the spectra. The beam energy is 20 meV, and the sample temperature is 300 K.

corresponding to an almost complete Cu-intercalated Gr surface, that is, Gr/Cu(0.7 ML)/Ru, compared to the one measured from pristine Gr/Ru(0001). As reported previously,[8,22] the Gr/Ru(0001) diffraction pattern presents several diffraction peaks due to the moiré reconstruction, labeled as $m(n,0)$. Within the experimental resolution, the periodicity of the moiré superstructure is 12-times larger than the atomic periodicity of Gr and 11-times larger than the Ru periodicity. Therefore, the $m(12,0)$ peak appears at the same angular position than the Gr(1,0) diffraction peak, whereas the $m(11,0)$ peak of the Gr covered sample coincides with the first order diffraction peak of the clean Ru(0001) surface.[23]



DOI: 10.1021/acs.nanolett.5b02887
Nano Lett. XXXX, XXX, XXX−XXX

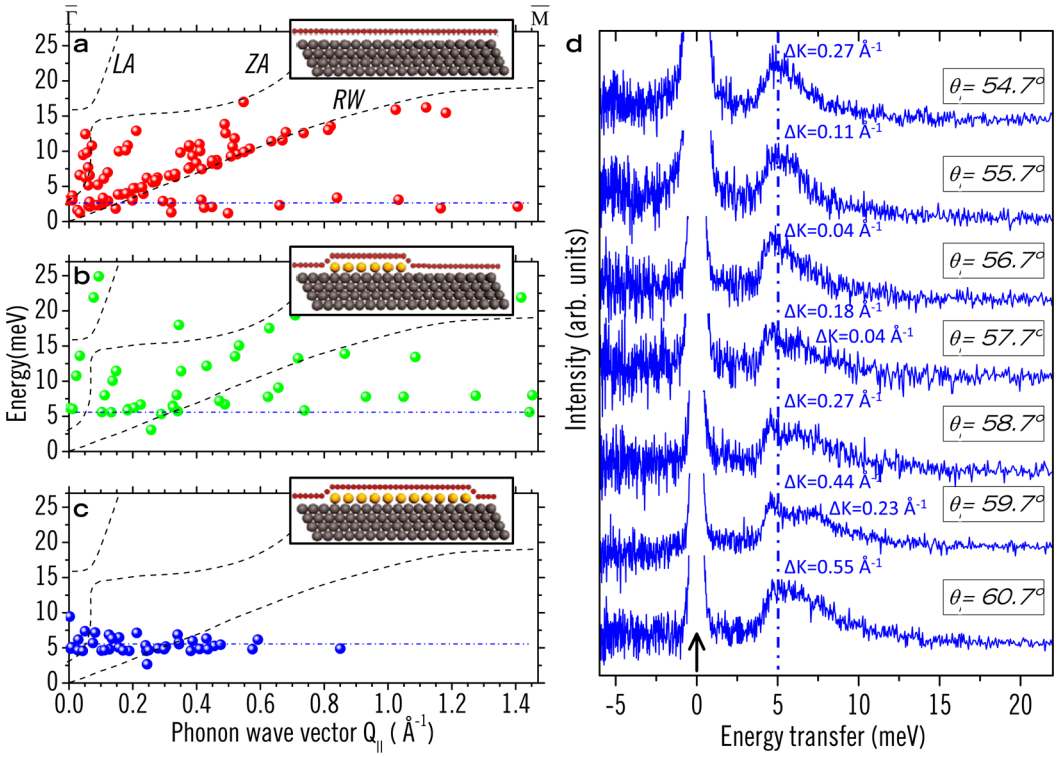


**Figure 3.** Experimentally determined surface phonon dispersion curves for (a) Gr/Ru(0001), (b) Gr/Cu(0.4 ML)/Ru(0001), and (c) Gr/Cu(0.7 ML)/Ru(0001). The dotted lines represent the Gr modes obtained from DFT calculations for Gr/Ru(0001).[23] (d) Representative inelastic HAS spectra measured along $\bar{\Gamma}\,\bar{M}$ for the intercalated Gr/Cu(0.7 ML)/Ru sample at $E_i$ = 21 meV and $T_S$ = 300 K for different incident angles. The arrow indicates the zero of energy scale.

The spectrum shown on the bottom of Figure 2 corresponds to the Gr/Cu(0.7 ML)/Ru(0001) surface. Diffraction peaks corresponding to the moiré periodicity, such as $m$(1,0) and $m$(2,0), are clearly resolved in the spectrum. This indicates, in agreement with the STM observations, that an ordered Gr layer is covering the Cu-intercalated surface, that is, that the structural order of Gr is preserved once the intercalation process has been performed. Furthermore, the lateral periodicity of the moiré superstructure is identical to the one of pristine Gr/Ru(0001). Notice that the $m$(11,0) and $m$(12,0) peaks are much smaller on the intercalated system, indicating that the surface corrugation (which is proportional to the ratio $m(12,0)/m(1,0)$) is much lower for the Cu intercalated system than for the Gr/Ru(0001) surface. Figure 2 shows that there is a great deal of nondiffractive scattering in the vicinity of the specular peak for the Gr/Cu(0.7 ML)/Ru(0001) spectrum. This large background points to the presence of a larger density of defects in the Cu-intercalated Gr film. This observation is consistent with the STM results shown in Figure 1, panel c.

The surface arising from the Cu intercalation treatment resulted to be inert and stable thermally up to 980 K. In fact, the HAS spectrum was found to remain unchanged after the sample was kept in UHV for one month, followed by thermal annealing up to 700 K. The same result has been reported for clean Gr/Ru(0001) samples, so it can be concluded that the top layer is composed of a well-ordered, intact Gr layer lying on top of the intercalated Cu regions.

The Gr layers grown directly on Ru(0001) and the ones obtained after Cu-intercalation have been examined by means of inelastic He scattering. Figure 3, panels a–c show the surface phonon dispersion curves determined from the measured time-of-flight (TOF) spectra along $\bar{\Gamma}\,\bar{M}$ for Gr/Ru(0001), Gr/Cu(0.4 ML)/Ru(0001), and Gr/Cu(0.7 ML)/Ru(0001) surfaces. The phonon branches measured for Gr/Ru(0001) (red dots) include three dispersive modes: the surface Rayleigh wave (RW) and the longitudinal (LA) and perpendicular (ZA) acoustic modes similar to those observed on graphite and described in detail elsewhere,[23] plus a puzzling branch of low energy dispersionless excitations.

To unravel the origin of this low energy mode, the intercalated surfaces, made of monolayer-high Cu islands embedded between the Gr monolayer and the Ru(0001) substrate, have been examined. For an almost completely Cu-intercalated surface, a radical modification of the phonon dispersion modes is observed in Figure 3, panel c: the dispersive branches characteristic of epitaxial Gr on Ru(0001) are no longer detectable. Notice, in particular, that the Rayleigh wave, which is clearly visible on Gr/Ru(0001), has completely disappeared on the Gr/Cu(0.7 ML)/Ru(0001) surface. Figure 4 shows two TOF spectra recorded under identical conditions for Gr/Ru(0001) (red curve) and Gr/Cu(0.7 ML)/Ru(0001) (blue curve). Notice that the Rayleigh wave is clearly visible in the red curve at ~12.5 meV (corresponding to $\Delta K = 0.66$ Å$^{-1}$), while it does not appear in the Cu-intercalated sample. The low-energy, dispersionless loss at 4–5 meV, however, is seen in both cases. The disappearance of the Rayleigh wave could be due to a lack of structural order of the Gr surface and a massive introduction of defects created by the intercalation process, but the presence of clear diffraction features in the spectrum shown on the bottom of Figure 2 proves that this is not the case. The absence of a Rayleigh wave on a well-ordered surface is a quite unusual result that points to a drastic weakening of the bonding interaction with the substrate produced by the intercalation of Cu in Gr/Ru(0001), which decouples the Gr layer from its


DOI: 10.1021/acs.nanolett.5b02887
Nano Lett. XXXX, XXX, XXX–XXX

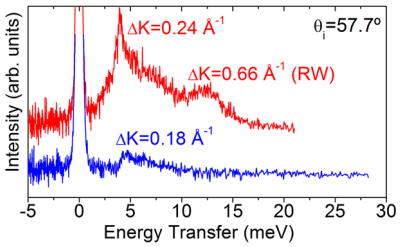


**Figure 4.** Comparison of TOF spectra recorded from Gr/Ru(0001) (red) and Gr/Cu(0.7 ML)/Ru(0001) (blue) under the same incident conditions ($E_i$ = 21 meV). The mode at 5 meV is present in both spectra, whereas the one corresponding to the Rayleigh wave (RW) at 12.5 meV is only detected from the Gr/Ru(0001) surface.

strong bond with Ru(0001). Similar weakening of the coupling of Gr to the substrate has been reported for Cu and Ag intercalation on Gr/Ni(111).[10,11]

The other modes characteristics of Gr/Ru(0001) have all disappeared as well, and only the low-energy, dispersionless mode remains. The direct experimental evidence of the existence of this mode is shown in Figure 3, panel d, where representative TOF spectra converted to energy-transfer scale for a Gr/Cu(0.7 ML)/Ru sample are shown. In this case, a prominent vibrational mode appears at about 5 meV. Notice that it does not disperse with increasing angle of incidence, that is, in a wide ($\Delta K$ = 0.04−0.55 Å$^{-1}$) range of values momentum transfer.

For the surface with partial Cu-intercalation (i.e., Gr/Cu(0.4 ML)/Ru), a coexistence of the phonon modes corresponding to the pristine Gr/Ru(0001) and the Cu-intercalated surface is observed. In effect, the data shown in Figure 3, panel b (green dots) reveal energy-transfer processes belonging to phonon dispersion branches recorded for pristine Gr/Ru(0001) (and graphite) plus a dispersionless-like branch at energy of about 5−7 meV, similar to the one observed on the Gr/Cu(0.7 ML)/Ru surface (blue dots). This is in agreement with the morphology revealed by STM (Figure 1), where there is a coexistence of intercalated and nonintercalated regions over which the Gr layer extends continuously. Therefore, the elastically scattered intensity, as well as the corresponding TOF spectra, will contain a superposition of the contributions from both regions of Gr.

The nanostructured nature of Gr/Ru(0001) and Cu-intercalated Gr/Ru(0001) resides behind the low-energy dispersionless mode detected in the TOF spectra. We propose that the presence of such a surface vibrational mode may be due to a collection of locally vibrating bodies whose energy motion is not transferred to each other. The self-organized array of hills and valleys, with a lateral periodicity of 0.30 nm, might be thought, in a simplified way, as a sort of flat "bubble wrap" foil made of a periodic arrangement of nanodomes anchored to the substrate and independent of each other. Such a concept can be better figured out by looking at Figure 5, panel a.

It is well-known that the strength of the C−Ru interaction varies strongly within the moiré unit cell of Gr/Ru(0001).[24,25] In the valley site, there is a strong bond between carbon and Ru atoms with a C−Ru distance of 0.214 nm almost identical to the sum of the covalent radii of C and Ru.[25] On the other hand, in the hill site, where the ring of the carbon atoms lie on top of a Ru atom, the interaction is much weaker and mostly due to van der Waals forces, and the C−Ru distance is 0.30 nm.[25] Thus, in first approximation, it can be assumed that the

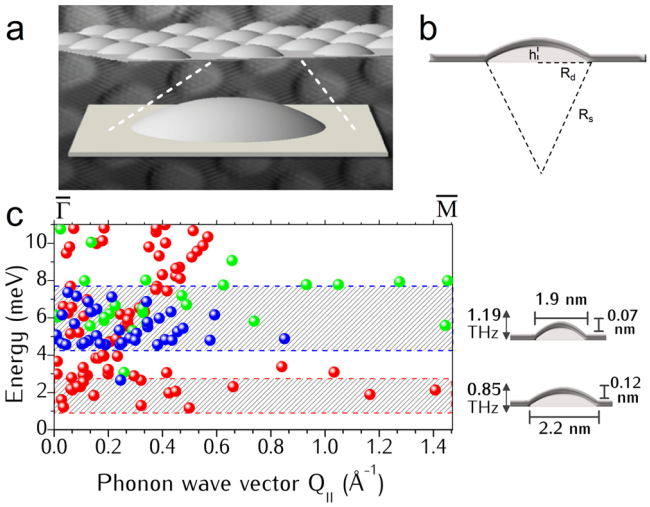


**Figure 5.** (a) The periodically rippled surface of Gr/Ru(0001) and Cu-intercalated visualized as a periodic array of nanodomes mechanically independent of each other. The picture in the background shows a real STM image, plus an schematic flat "bubble wrap" foil, where the structure of a single nanodome is further amplified. (b) Vertical section of the nanodome model, defined by the height ($h$), the radius of the base of the dome ($R_d$), and the radius of the corresponding sphere ($R_s$). (c) Energy dispersion of the low-energy inelastic HAS data from Gr/Ru(0001) and Gr/Cu/Ru (0001) surfaces. The dark regions mark the energy ranges corresponding to the data points for pristine Gr/Ru(0001) (red) and Cu-intercalated Gr/Ru(0001) (green and blue) samples, respectively. The experimental data follow the trend predicted by eq 1 for the different sizes of the nanodomes. Note that some data points corresponding to the Gr/Ru(0001) nanodomes are detected from the Cu-intercalated surface, as expected from the coexistence of clean Gr/Ru(0001) areas with intercalated ones revealed by the STM images (Figure 1).

nanodome, formed by the Gr hill, is rigidly anchored to the substrate on the valley sites. In contrast, in the hill site, the Gr nanodome freely vibrates at characteristic eigen-frequencies determined by its structure and size. Moreover, it has been shown that the deformation of such nanodomes is reversible and does not affect the vibrational status of its neighbors.[26] Although at the nanoscale the use of continuum mechanics is arguable,[27] it is reasonable to estimate the natural frequency for a dome, with a structure such as that shown in Figure 5, panel b, by using the shallow shell theory.

It can be demonstrated that the natural frequency of a shallow spherical shell ($f_{shell}$) is related to the corresponding frequency of a flat plate ($f_{plate}$) corresponding to its projection by the following equation:[28]

$$f_{shell} = \sqrt{{f_{plate}}^2 + \frac{E}{4\pi^2 \rho {R_S}^2}} \quad (1)$$

where $E$ is the Young's modulus, $\rho$ the mass density of the material, and $R_s$ is the radius of curvature of the shell. From continuum mechanics,[29] it is well-known that $f_{plate} = (\lambda/2\pi {R_d}^2)\sqrt{Et^2/12\rho(1-\nu^2)}$, where $R_d$ is the radius of the plate, $t$ its thickness, $\nu$ the Poisson's ratio, and the parameter $\lambda$ depends on the boundary conditions. If the edge of the plate is clamped, $\lambda$ = 10.22, independently of the value of $\nu$.

The choice of the parameter values, in the case of Gr, is not trivial and is currently a matter of debate. According to molecular mechanics calculations by Gupta et al.,[30] the elastic


DOI: 10.1021/acs.nanolett.5b02887
Nano Lett. XXXX, XXX, XXX−XXX

response of a Gr monolayer under normal stress is comparable to that of a thin slab with $E$ = 3.4 TPa, $\nu$ = 0.21, $t \approx 0.1$ nm, and $\rho$ = 8561 kg/m$^3$ (well-above the mass density of graphite). Introducing these values in eq 1 together with $R_d$ = 1.1 nm and $R_s$ = 10.2 nm (as estimated from the shell height $h$ = 0.12 nm), we estimate a resonance frequency $f_{shell} \approx 0.85$ THz, which is only slightly larger than the frequency $f_{plate} \approx 0.79$ THz of the corresponding plate. Note that, with the same parameter values, the normal stiffness $k \approx 16\pi Et^3/3\ R_d^2$ = 47 N/m is in good agreement with recent density functional theory (DFT) calculations by Stradi et al., according to which $k$ = 44 N/m.[26] The corresponding vibrational energy of the shell is 3.5 meV. This model is very sensitive to the size of the nanostructures involved. For instance, by reducing the radius of the base by 15%, eq 1 returns a vibration energy of about 4.9 meV (i.e., 1.19 Thz). On the other side, the shape of the nanodomes has only a slight influence on the value of $f_{shell}$. Indeed, the resonance frequency of a flat square plate differs by a factor of 1.12 only from the value of $f_{plate}$ for a circular plate with the same area.[29] Since the Gr nanodomes are only slightly curved, we do not expect a significant change of frequency for a shallow shell with square basis (for which a simple analytical formula is not available). The differences will be even less appreciable for geometric shapes resembling the Gr nanodomes, which appear overall more rounded than a square-based shell.

Both the STM and HAS results reveal that the periodicity (and its characteristic hexagonal arrangement) of the moiré pattern is preserved after intercalating Cu atoms, but its structure appears slightly modified and resized, as demonstrated by the STM profiles in Figure 1, panel c. In spite of the overall weaker C−Cu bonding as compared to C−Ru, the similar moiré pattern and the pseudomorphic nature of the Cu layer imply substantial differences in the C−Cu bonding on hills and valleys, justifying the use of the same mechanical model for the Gr/Cu/Ru(0001) system. This information (smaller dome radius and height for Cu-intercalated Gr), together with the observed distribution of sizes in both cases, has been put into eq 1 to estimate the frequencies corresponding to the pristine and Cu-intercalated Gr surface. The values obtained are shown as dark regions in Figure 5, panel c. In spite of the simplicity of the model, it provides a satisfactory description of the data.

Although alternative explanations, for example, vibrations localized in defects introduced by the intercalation process, might be possible, we tend to favor the one presented above, since the low-energy losses are present on the pristine Gr/Ru(0001) system where the number of defects is negligible. We have illustrated this point by studying the low-energy excitations of Gr epitaxially grown on Ru(0001), a well characterized system that presents a spontaneous, periodic arrangement of nanodomes. The nature of a branch of ultra low energy, dispersionless inelastic losses observed has been clarified by intercalation of Cu below the Gr monolayer on Ru(0001). He-diffraction proves that the Cu intercalated Gr layer possesses an excellent degree of structural long-range order, while STM reveals the presence of the (slightly modified) array of Gr nanodomes. The images further demonstrate that the Gr overlayer extends continuously over the different areas. The intercalation of Cu decouples the Gr layer from the Ru substrate and eliminates most of the Gr-related modes, such as the Rayleigh wave, leaving only the dispersionless one.

These results suggest that the observed dispersionless mode is the result of a collection of entities, that is, the Gr nanodomes, vibrating independently at a characteristic frequency. A simple mechanical model has been proposed to explain the origin of this low-energy mode, which provides a good interpretation of the experimental data. According to this, the detected energy transfer to the scattered He atoms corresponds to the natural frequencies of the nanodomes, which are determined by the material and size of the nanostructures. The latter depends, in turn, on the interactions between the Gr layer and the substrate. Therefore, by choosing the appropriate element to intercalate, it is possible to change the size and shape of the domes and, consequently, modify the resonance frequency range and the mechanical response. This uncommon mechanical response, where a localized vibration is present and the Rayleigh wave disappears, might be exploited to control the heat transport in intercalated Gr.[4,5]

## ■ ASSOCIATED CONTENT

### Supporting Information

The Supporting Information is available free of charge on the ACS Publications website at DOI: 10.1021/acs.nanolett.5b02887.

STM images showing the early stages of Cu intercalation and atomic resolution of Gr/Ru and Gr/Cu/Ru nanodomes; atomic resolution STM image of Cu/Ru(0001); inelastic HAS−TOF spectra recorded from the intercalated Gr/Cu(0.4 ML)/Ru sample (PDF)

## ■ AUTHOR INFORMATION


### Corresponding Author

*E-mail: daniel.farias@uam.es. Phone: +34 91 497 5550.



### Funding

This work has been supported by projects FIS 2013-40667-P, MAT2012-39308 of Spanish MINECO, S2013/MIT-3007 (MAD2D-CM), S2013/MIT-2850 (NANOFRONTMAG-CM) of Comunidad de Madrid and by the European Union, FP7: Theme NMP.2012.1.4-3, Grant no. 309672. P.P. acknowledges support through the Marie Curie AMAROUT EU Programme and through MINECO JCI-2011-09602.


### Notes

The authors declare no competing financial interest.

## ■ REFERENCES


(1) Stipe, B. C.; Rezaei, M. A.; Ho, W. *Science* **1998**, *280*, 1732−1735.
(2) Jarvis, S. P.; Yamada, H.; Yamamoto, S. L.; Tokumoto, H.; Pethica, J. B. *Nature* **1996**, *384*, 247−249.
(3) Heinrich, A. J.; Gupta, J. A.; Lutz, C. P.; Eigler, D. M. *Science* **2004**, *306*, 466−469.
(4) Balandin, A. A.; Ghosh, S.; Bao, W.; Calizo, I.; Teweldebrhan, D.; Miao, F.; Lau, Ch. N. *Nano Lett.* **2008**, *8*, 902−907.
(5) Seol, J. H.; Jo, I.; Moore, A. L.; Lindsay, L.; Aitken, Z. H.; Pettes, M. T.; Li, X.; Yao, Z.; Huang, R.; Broido, D.; Mingo, N.; Ruoff, R. S.; Shi, L. *Science* **2010**, *328*, 213−216.
(6) Toennies, J. P. *Surface Phonons*; Springer: Berlin-Heidelberg, 1991.
(7) Vázquez de Parga, A. L.; Calleja, F.; Borca, B.; Passeggi, M. C. G.; Hinarejos, J. J.; Guinea, F.; Miranda, R. *Phys. Rev. Lett.* **2008**, *100*, 056807.
(8) Borca, B.; Barja, S.; Garnica, M.; Minniti, M.; Politano, A.; Rodríguez-Garcia, J. M.; Hinarejos, J. J.; Farías, D.; Vázquez de Parga, A. L.; Miranda, R. *New J. Phys.* **2010**, *12*, 093018.




DOI: 10.1021/acs.nanolett.5b02887
*Nano Lett.* XXXX, XXX, XXX−XXX

(9) Pan, Y.; Zhang, H.; Shi, D.; Sun, J.; Du, S.; Liu, F.; Gao, H.-J. *Adv. Mater.* **2009**, *21*, 2777−2780.
(10) Shikin, A. M.; Farías, D.; Rieder, K. H. *Europhys. Lett.* **1998**, *44*, 44.
(11) Farías, D.; Shikin, A. M.; Rieder, K. H.; Dedkov, Y. S. *J. Phys.: Condens. Matter* **1999**, *11*, 8453.
(12) Otero, R.; Calleja, F.; García-Suárez, V. M.; Hinarejos, J. J.; de la Figuera, J.; Ferrer, J.; Vázquez de Parga, A. L.; Miranda, R. *Surf. Sci.* **2004**, *550*, 65−72.
(13) Calleja, F.; García-Suárez, V. M.; Hinarejos, J. J.; Ferrer, J.; Vázquez de Parga, A. L.; Miranda, R. *Phys. Rev. B: Condens. Matter Mater. Phys.* **2005**, *71*, 125412.
(14) Houston, J. E.; Peden, C. H. F.; Blair, D. S.; Goodman, D. W. *Surf. Sci.* **1986**, *167*, 427.
(15) Potschke, G. O.; Behm, R. J. *Phys. Rev. B: Condens. Matter Mater. Phys.* **1991**, *44*, 1442.
(16) Feibelman, P. J.; Houston, J. E.; Davis, H. L.; O'Neill, D. G. *Surf. Sci.* **1994**, *302*, 81.
(17) Gunther, C.; Vrijmoeth, J.; Hwang, R. Q.; Behm, R. J. *Phys. Rev. Lett.* **1995**, *74*, 754.
(18) Ruebush, S. D.; Couch, R. E.; Thevuthasan, S.; Fadley, C. S. *Surf. Sci.* **1999**, *421*, 205.
(19) Zajonz, H.; Baddorf, A. P.; Gibbs, D.; Zehner, D. M. *Phys. Rev. B: Condens. Matter Mater. Phys.* **2000**, *62*, 10436.
(20) de la Figuera, J.; Schmid, A. K.; Bartelt, N. C.; Pohl, K.; Hwang, R. Q. *Phys. Rev. B: Condens. Matter Mater. Phys.* **2001**, *63*, 165431.
(21) Calleja, F.; García-Suárez, V. M.; Hinarejos, J. J.; Ferrer, J.; Vázquez de Parga, A. L.; Miranda, R. *Phys. Rev. B: Condens. Matter Mater. Phys.* **2005**, *71*, 125412.
(22) Shichibe, H.; Satake, Y.; Watanabe, K.; Kinjyo, A.; Kunihara, A.; Yamada, Y.; Sasaki, M.; Hayes, W. W.; Manson, J. R. *Phys. Rev. B: Condens. Matter Mater. Phys.* **2015**, *91*, 155403.
(23) Maccariello, D.; Campi, D.; Al Taleb, A.; Benedek, G.; Farías, D.; Bernasconi, M.; Miranda, R. *Carbon* **2015**, *93*, 1.
(24) Stradi, D.; Barja, S.; Díaz, C.; Garnica, M.; Borca, B.; Hinarejos, J. J.; Sánchez-Portal, D.; Alcamí, M.; Arnau, A.; Vázquez de Parga, A. L.; Miranda, R.; Martín, F. *Phys. Rev. Lett.* **2011**, *106*, 186102.
(25) Stradi, D.; Barja, S.; Díaz, C.; Garnica, M.; Borca, B.; Hinarejos, J. J.; Sánchez-Portal, D.; Alcamí, M.; Arnau, A.; Vázquez de Parga, A. L.; Miranda, R.; Martín, F. *Phys. Rev. B: Condens. Matter Mater. Phys.* **2013**, *88*, 245401.
(26) Koch, S.; Stradi, D.; Gnecco, E.; Barja, S.; Kawai, S.; Díaz, C.; Alcamí, M.; Martín, F.; Vázquez de Parga, A. L.; Miranda, R.; Glatzel, T.; Meyer, E. *ACS Nano* **2013**, *7*, 2927−2934.
(27) Tapasztó, L.; Dumitrica, T.; Kim, S. J.; Nemes-Incze, P.; Hwang, C.; Biró, L. *Nat. Phys.* **2012**, *8*, 739−742.
(28) Schiff, D. *Dynamic Analysis and Failure Modes of Simple Structures*; Wiley-Interscience, 1990.
(29) Landau, L. D.; Lifshitz, L. M. *Theory of Elasticity*; Butterworth-Heinemann, 1986.
(30) Gupta, S. S.; Batra, R. C. *J. Comput. Theor. Nanosci.* **2010**, *7*, 2151−2164.



DOI: 10.1021/acs.nanolett.5b02887
*Nano Lett.* XXXX, XXX, XXX−XXX